Thermo-Resistant Soft Glassy Suspensions of Polymeric Micellar Nanoparticles in Ionic Liquid

Sandra Gkermpoura,[†] Marc Obiols-Rabasa,[‡] Zacharoula Iatridi,[†] and Constantinos Tsitsilianis*,[†,§]

[†]Department of Chemical Engineering, University of Patras, 26504 Patras, Greece
[‡]Division of Physical Chemistry, Department of Chemistry, Lund University, SE-221 00 Lund, Sweden
[§]Institute of Chemical Engineering Sciences (ICEHT/FORTH), 26504 Patras, Greece

S *Supporting Information*

ABSTRACT: We report the rheological and structural properties of a suspension comprising poly(ethylene oxide)−polystyrene−poly(ethylene oxide) core−shell micellar nanoparticles dispersed in 1-butyl-3-methylimidazolium hexafluorophosphate ionic liquid. A liquid to soft solid transition was observed at a copolymer concentration of 10 wt % above which an elastic soft material was formed, which was composed of non-ordered jammed core−shell micellar nanoparticles. In the soft solid state, a significant reduction in the size of the nanoparticles, approaching hard sphere behavior, was observed by small-angle X-ray scattering which is attributed to compression of the soft poly(ethylene oxide) coronas. The nonvolatile ionic liquid-based glassy soft solid formed exhibited remarkable thermal stability with a melting temperature of 141 °C at 20 wt % copolymer, which renders it suitable for applications involving elevated temperatures and/or reduced pressure where water-based formulations are inappropriate.

KEYWORDS: *block copolymer nanoparticle, ionic liquid, jamming, soft colloidal glass, rheological properties, thermal stability*
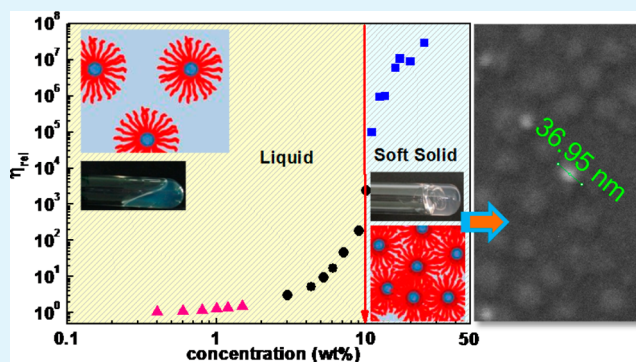
■ INTRODUCTION

Soft solids formed by block copolymers in selective solvent suspensions comprised of solvophilic and solvophobic segments covalently bonded in various topologies have attracted increasing interest over the last couple of decades. This is attributable to the unique properties they exhibit and their ability to be used in a wide range of applications as rheology modifiers in many advanced technologies.[1−5] Two types of polymeric soft solids have been studied to date: those arising from intermolecular interactions (mainly solvophobic) that lead to the formation of a transient three-dimensional network above a certain percolation threshold (known as physical gels)[6−9] and those arising from jamming of close-packed micellar nanoparticles (in the absence of bridges) under conditions of high-volume fractions in which the ability of the system to flow is lost.[10] The later behavior is also found in suspensions of other colloidal nanoparticles that form colloidal glasses, like microgels, inorganic silica nanoparticles, surfactant-type micelles, multi-armed star-shaped polymers, and so forth.[11−17]

Free-supporting physical gels have been developed in various media, from organic solvents to water, as well as in ionic liquids (ILs). Among them, aqueous media hosting amphiphilic macromolecules of various architectures in which a rich pallet of interactions can be activated between associative segments have attracted major interest. Recently ILs consisting of ions (molten salts), also promoted as "green solvents", have attracted considerable attention as media in various fields of chemistry due to unique properties they possess, including nonflammability, negligible vapor pressure, high ion conductivity, thermal and chemical stability, and so forth.[18−21]

As far as polymer/IL gels (also termed ion gels) are concerned, the primary motivation for their development is the high ionic conductivity they exhibit, which makes them attractive soft materials with interesting applications as solid or quasi-solid electrolytes for electrochemical devices like lithium ion batteries, fuels, and solar cells.[22−24] Owing to the fact that segmented polymers (block copolymers) can be tuned precisely through macromolecular engineering[25] and that the solvation properties of ILs can be designed based on the choice of the chemical structure of the employed ions (cations/anions), polymer/IL complex fluids appear to have many advantages and to be promising systems.[26,27]

The first physically cross-linked ion gel reported was prepared by a polystyrene−poly(ethylene oxide)−polystyrene (PS−PEO−PS) triblock copolymer in 1-butyl-3-methylimida-

zolium hexafluorophosphate ($[BMIM][PF_6]$).[28] Because of the solvophobic PS end-blocks and a solvophilic PEO midblock, the copolymer self-assembled to form a transient network above 5 wt % polymer.[28−30] In the same context, other copolymer/IL systems that form transient ion gels with interesting rheological properties, including thermoresponsiveness, have been explored.[31−34] Ion gels seem to be promising soft materials as solid or quasi-solid electrolytes for electrochemical devices.[35−38]

Colloidal systems involving silica nanoparticles grafted with polymeric chains have also been employed to prepare IL-based solidlike soft materials.[39−41] Furthermore, highly concentrated suspensions of poly(benzyl methacrylate) (PBnMA)-grafted silica nanoparticles in $[EMIM][TFSA]$ formed soft glassy colloidal arrays that exhibited soft solid behavior. On the basis of the thermosensitivity of the PBnMA-grafted chains, the interparticle interactions changed from repulsive to attractive above the lower critical solution temperature (LCST), which induced a colloidal glass-to-gel transition marked by a V-shaped rheological response.[41]

Although much work has been reported on ion gels arising from the physical bridging of ABA triblock copolymers, to the best of our knowledge, there are no reports addressing jamming systems. In this work, we explore rheological and structural behavior as a function of suspension concentration of polymeric nanostructured micelles formed by PEO−PS−PEO triblock copolymers in $[BMIM][PF_6]$. In contrast to the differing topology (BAB versus ABA), the chemical nature of the components involved (i.e., solvophobic/solvophilic blocks, IL) is kept the same as those of ion gels previously reported[28,30] for the sake of comparison. Because of the solvophobic nature of PS in $[BMIM][PF_6]$, the triblock self-assembles to form spherical, hairy micelles with compact PS cores and soft PEO swollen coronas. At elevated concentrations, the micelles jam, forming a soft glassy solid with structural and rheological properties that are significantly different from those reported for the PS−PEO−PS counterpart and with remarkable thermal stability. Ionic liquid-based colloidal glassy suspensions could be used in applications under special conditions (e.g., high temperatures or under vacuum) where water-based colloids are not suitable. Because of the high ionic conductivity of the medium, this kind of soft solid could also have applications in electrochemical devices.

■ EXPERIMENTAL SECTION

Materials. $[BMIM][PF_6]$ was purchased from Alfa Aesar. All other reagents used for the synthesis and sample preparation were purchased from Merck.

Polymer Synthesis and Characterization. The triblock copolymer PEO−PS−PEO was synthesized through living anionic polymerization under an argon atmosphere by sequential addition of the monomers (styrene, oxirane) using potassium naphthalene as the difunctional initiator according to standard procedures.[42] The molecular weight and composition characteristics of the triblock copolymer were determined using static light scattering (SLS), gel permeation chromatography (GPC), and proton nuclear magnetic resonance (^{1}H NMR) (Supporting Information). In Table 1, the weight-averaged molecular weight, M_w, the polydispersity index (M_w/M_n), and the chemical composition of the triblock copolymer are presented.

Sample Preparation. Polymer dispersions in an IL were prepared by mixing weighted amounts of the copolymer with methylene chloride (CH_2Cl_2) as the polymer/IL cosolvent. To those homogeneous solutions was added an appropriate amount of IL under vigorous stirring. The viscous samples were homogenized

Table 1. Molecular Characteristics of the PEO−PS−PEO Triblock Copolymer

		PS block			PEO blocks		
$M_w{}^a$	$M_w/M_n{}^b$	$M_{w(PS)}$	wt %^{c}	DP_{PS}	$M_{w(PEO)}$	wt %^{c}	DP_{PEO}
82210	1.25	29850	36.3	287	26180	63.7	595

^{a}Determined by SLS. ^{b}Determined by GPC. ^{c}Determined by ^{1}H NMR.

several times by centrifugation of the vials. Finally, the cosolvent was removed by placing the samples in a vacuum oven at 70 °C until a constant weight was achieved.

Dynamic Light Scattering (DLS). Autocorrelation functions $g(q,t)$ were measured with a BI-9000AT/Turbocorr digital correlator from a He−Ne laser (wavelength 632.8 nm) light source. CONTIN analysis was performed through BI-DLSW software. The apparent hydrodynamic radius, $R_{h,app}$, was determined via the Stokes−Einstein equation (eq 1).

$$R_{h,app} = \frac{k_B T}{6\pi\eta D} \tag{1}$$

where $D = \Gamma/q^2$ is the diffusion coefficient of the scattered dispersed particles, k_B is the Boltzmann constant, and η is the viscosity of the solvent at 25 °C. A 0.8 wt % PEO−PS−PEO/$[BMIM][PF_6]$ solution was prepared for the DLS experiments. The solution was passed through a 0.45 μm filter and allowed to equilibrate at room temperature for 24 h.

AMVn Microviscometer. The viscosity of the polymer solutions in a concentration range of 0.4−1.5 wt % was measured according to Höppler's "falling ball" principle. The solutions were introduced into a glass capillary containing a rolling steel ball (diameter 3 mm), and the viscosity was determined by measuring the rolling time of the ball over a fixed capillary distance. The measurement was performed at a constant angle of 20°. The intrinsic viscosity, $[\eta]$, was determined using Fedors equation (eq 2).[43]

$$\frac{1}{2(\sqrt{\eta_{rel}} - 1)} = \frac{1}{C[\eta]} - \frac{1}{C_m[\eta]} \tag{2}$$

where η_{rel} is the relative viscosity and C_m is a polymer concentration parameter.

Small-Angle X-ray Scattering (SAXS). Small-angle X-ray scattering measurements were performed using the SAXSLab Ganesha 300XL instrument (SAXSLAB ApS, Skovlunde, Denmark), a pinhole-collimated system equipped with a Genix 3D X-ray source (Xenocs SA, Sassenage, France). Data was collected with the detector placed at two sample-to-detector positions that yielded to an overall q range of 0.005−0.15 Å^{-1}. The magnitude of the scattering vector is defined as $q = (4\pi/\lambda)\sin(\theta)$, where λ corresponds to the X-ray wavelength (1.54 Å) and θ is half of the scattering angle. Samples were sealed at room temperature between two kapton windows in a metallic block. The most diluted sample, e.g., 0.1 wt %, was placed in a 1.5 mm diameter quartz capillary (Hilgenberg GmbH, Malsfeld, Germany). In all cases the temperature was kept at 23 ± 0.2 °C by an external recirculating water bath. The two-dimensional (2D) scattering pattern was recorded using a 2D 300 K Pilatus detector (Dectris Ltd., Baden, Switzerland) and radially averaged using SAXSGui software to obtain $I(q)$. The measured scattering curves were corrected for kapton scattering and fitted using SasView software. SAXS data were fitted using different models depending on the sample concentration. For the lowest concentration (0.1 wt %), a form factor of spheres with a core−shell structure[44] was used (eq 3).

$$P(q) = \frac{I_0}{V_s}\left[3V_c(\rho_c - \rho_s)\frac{[\sin(qR_c) - qR_c\cos(qR_c)]}{(qR_c)^3}\right.$$

$$\left. + 3V_s(\rho_s - \rho_{solv})\frac{[\sin(qR_s) - qR_c\cos(qR_s)]}{(qR_s)^3}\right]^2$$

$$+ I_{bg} \tag{3}$$

where I_0 is the scaling factor, V_s is the volume of the outer shell, V_c is the volume of the core, R_c is the radius of the core, R_s is the radius of the shell, ρ_c, ρ_s, and ρ_{solv} are the scattering length densities of the core, shell, and solvent, respectively, and I_{bg} is the background level. The values for ρ_c and ρ_{solv} were kept equal to 2.10^{-6} and 1.10×10^{-6} Å^{-2}, respectively, throughout the fitting process.

The polydispersity of the system accounted for a radius of the core having a Gaussian distribution (eq 4).

$$f(x) = \frac{1}{\sigma\sqrt{2\pi}}\exp\left[-\frac{1}{2\sigma^2}(r - r_{avg})^2\right] \tag{4}$$

where r_{avg} is the average radius and the polydispersity is given by σ/r_{avg}.

For concentrations between 1 and 5.5 wt %, the SAXS curves were fitted with a form factor for a sphere with a core−shell structure (eq 3) and a radius of the core with a Gaussian distribution (eq 4), together with a hard sphere structure factor.[45]

For concentrations ≥9 wt %, a form factor for homogeneous spheres[44] (eq 5) together with a hard sphere structure factor was used.

$$P(q) = \frac{I_0}{V}\left[\frac{3V(\Delta\rho)(\sin(qR) - qR\cos(qR))}{(qR)^3}\right]^2 + I_{bg} \tag{5}$$

where V is the volume of the sphere, $\Delta\rho$ is the difference of the scattering length density between the solvent and particle (kept constant and equal to 1.10^{-6} Å^{-2}), and R is the radius of the sphere, which corresponds to the radius of the core plus that of the collapsed shell ($R = R_c + R_s$). The structural parameters obtained from fitting of the SAXS curves are shown in Table S1 (Supporting Information).

Rheology. Rheological experiments were performed on a stress-controlled rheometer (AR-2000ex, TA Instruments) using a cone plate geometry (diameter = 20 mm, cone angle = 4°, truncation = 111 μm). Special care was taken during sample loading to exclude bubbles. After loading, a delay of 5 min was applied prior to any measurements. The rheometer was equipped with a Peltier control system that allows for accurate control of temperature. The linear viscoelastic regime was established by oscillatory strain sweeps using a frequency of 1 Hz. Dynamic shear moduli (G' and G'') were examined in the linear viscoelastic regime at 25 °C. Steady shear measurements were similarly made at 25 °C by increasing the shear stress stepwise and allowing for equilibrium to be reached at each step for 3 min. Dynamic temperature ramps were performed for 20 wt % PEO−PS−PEO in [BMIM][PF$_6$]. These measurements were also performed using parallel plate geometry calibrated to take into account thermal expansion of the tool at a strain amplitude of 1%, frequency of 1 Hz, and heating rate of 1 °C/min.

Scanning Electron Microscopy (SEM). SEM was performed using an FEI QUANTA FG 250 scanning electron microscope. The sample was prepared by placing a small amount of the 20 wt % soft solid (ion gel) on a mica substrate and subsequently rinsing with dichloromethane to remove IL. The specimen was sputtered with gold before imaging.

■ RESULTS AND DISCUSSION

Nanoparticle Characterization and Overlapping Concentration. Because of the selectivity of the solvent (i.e., bad for PS and good for PEO),[28] the PEO−PS−PEO triblock copolymer self-assembles in [BMIM][PF$_6$] to form core−shell micelles above a critical micelle concentration that was expected to be much lower than the concentration range investigated due to the long PS block. Moreover, because of the

high T_g of the insoluble block, "frozen" micelles were formed at temperatures below T_g (~100 °C), and therefore, these micelles will be referred to as micellar nanoparticles. Dynamic light scattering was utilized to estimate the size of the nanoparticles initially formed in dilute solutions. Figure 1
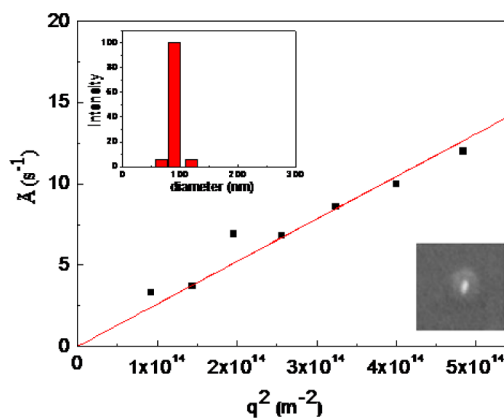

Figure 1. Decay rate (Γ) as a function of the square of the scattering vector (q) for a 0.8 wt % PEO−PS−PEO/[BMIM][PF$_6$] solution at 25 °C. Inset: particle size distribution obtained by CONTIN analysis of the autocorrelation function at an angle of 90°, and an image of a core−shell nanoparticle isolated from the SEM micrograph of Figure S3c (Supporting Information).

shows the decay rate as a function of the square of the scattering vector (q), which was deduced from the autocorrelation functions obtained from a 0.8 wt % solution at room temperature. The Γ/q^2 is practically independent of q, revealing a diffusive mode of the relaxation process that corresponds to nanoparticles with a mean apparent hydrodynamic radius R_h = 45 nm. Moreover, the particle size distribution is monomodal and narrow (Figure 1 inset), indicating low size polydispersity and a lack or negligible presence of unimers and micellar clusters. Given that the PS block length is considerably shorter than those of the outer PEO solvophilic blocks, spherical hairy nanoparticles were expected to be formed as verified by SEM (inset of Figure 1 and Figure S3, Supporting Information).

To evaluate the overlapping concentration of the micellar nanoparticles (c^*), viscometric studies were performed to determine the intrinsic viscosity [η]. For this purpose, the Fedors equation (eq 2) was used because it is quite suitable for associating amphiphilic copolymers.[46,47] Indeed, as shown in Figure 2, an excellent linear fit of the data was obtained, giving [η] = 18.32 g/g or 13.42 mL/g (d_{IL} = 1.365). The c^* was determined at ~8 wt % using the equation[48]

$$c^* = \frac{3x6^{3/2}\Phi}{4\pi N_A[\eta]} \tag{6}$$

where Φ is the Flory universal constant (2.5×10^{23}) and N_A is Avogadro's number.

Characterization by SAXS. Small-angle X-ray scattering measurements were performed to characterize the micelles formed upon self-assembly of PEO−PS−PEO, quantify the interactions between the micelles, and study the evolution of the micellar structure. The SAXS results are shown in Figure 3 for PEO−PS−PEO/IL suuspensions at concentrations between 0.1 and 5.5 wt % (Figure 3a) and between 9 and 24.8 wt %
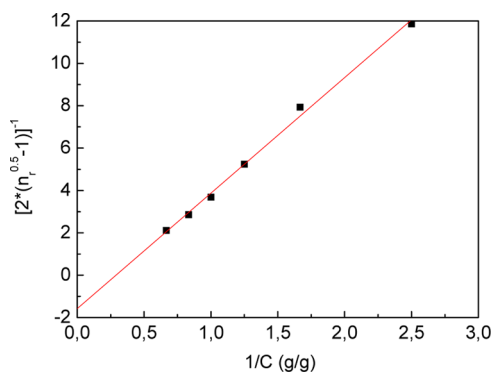
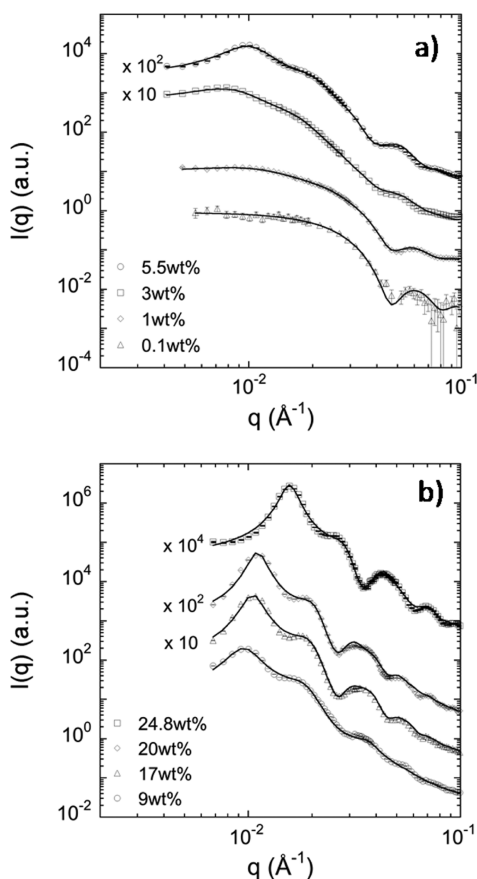**Figure 2.** Linear fit of the Fedors equation for the PEO−PS−PEO triblock copolymer dissolved in [BMIM][PF$_6$].

Figure 3. $I(q)$ vs q data obtained by SAXS for PEO−PS−PEO/[BMIM][PF$_6$] suspensions at concentrations of (a) 0.1, 1, 3, and 5.5 wt % and (b) 9, 17, 20, and 24.8 wt %. Solid lines are fits of the data as discussed in the text.

(Figure 3b). The results were split into two different plots in the same figure for clarity.

As shown in Figure 3, the sample at 0.1 wt % shows no intermicellar interactions, which is proven by the absence of a structure peak. Thus, the scattering curve corresponds to the form factor. The fitting of the curve yields a core radius (R_c) according to a similar approach reported by Lemmers et al. in their study on the transient network formation of flowerlike micelles.[49] The radius of the core, which corresponds to the size of the PS dense core, is found to be R_c = 10 ± 1 nm. The fitting also yields the radius of the shell (R_s), which is 11 ± 3 nm and corresponds to the size of the PEO soft corona. The

overall size of the micelle found from the fitting of the SAXS curves is therefore ∼21 ± 3 nm. This value is much smaller than the apparent hydrodynamic radius of the micelles (R_h = 45 nm) determined by DLS at 0.8 wt % in which a structure factor is slightly present (see curve corresponding to 1 wt % in Figure 3). However, the value from SAXS derived at 0.1 wt % might be underestimated based on the fact that the scattering predominantly arises from the core of the micelles.

Assuming that the PS core of the nanoparticles is not penetrated by the IL molecules, the aggregation number (N_{agg}) could be estimated by eq 7 using simple geometrical considerations.

$$\frac{4\pi}{3}R_c{}^3 = \frac{N_{agg}M_{n,PS}}{\rho_{PS}N_{av}} \tag{7}$$

where $M_{n,PS}$ is the number-average molecular weight of the PS block (23.88 kDa) and ρ_{PS} is the density of PS (1.05 g/cm^3). N_{agg} was found to be 88, which is reasonable with respect to the solvophobic/solvophilic balance of the copolymer.[50] Therefore, the spherical nanoparticles formed by the PEO−PS−PEO copolymer in the dilute regime are constituted of a PS core of R_c = 10 nm surrounded by a swollen corona of 176 PEO dangling chains. Thus, the grafting density of the nanoparticle core, as calculated from the formula $2N_{agg}/4\pi R_c{}^2$, is ∼0.14 chain/nm^2, implying chain extension of the corona chains. From the SAXS data, the degree of chain extension ($100R_s$/PEO contour length) was estimated to be 3.7%, whereas this value from the DLS data ($100(R_h−R_c)$/PEO contour length) was found to be 11.8%. The second value seems to be more consistent with respect to the 0.14 chain/nm^2 grafting density.[51] Given that PS is a glassy polymer, these "frozen" micellar nanoparticles seem to resemble poly(methyl methacrylate)-grafted silica nanoparticles (PMMA-g-NP) that form colloidal soft solids in ILs.[39−41]

For concentrations between 1 and 5.5 wt %, the R_c and R_s values remain the same as those obtained from the most diluted samples. This result is expected because these concentrations are below the overlapping concentration (c^*); thus, no compression of the shell is expected. At concentrations above c^* (e.g., ≥9 wt %), the micelles would be expected to start to overlap and/or collapse onto the core; thus, the shell contribution to the scattering data cannot be differentiated by SAXS. Therefore, the fitting of the SAXS data for these concentrations yields a radius (R) that corresponds to the sum of the radius of the core and that of the collapsed shell ($R = R_c + R_s$). The values of R obtained are ∼16 ± 3 nm.

The structuring of the samples is noticeable for samples with concentrations ≥1 wt %, which is revealed by the presence of a structure peak (see Figure 3). Thus, the SAXS data of these samples were fitted with a form factor together with a hard sphere structure factor, yielding an equivalent hard sphere radius (R_{HS}) and an equivalent hard sphere effective volume fraction (φ). As shown in Figure 4a, the position of the first structure peak (q^*) shifted towards higher q values with increasing concentration, indicating a decrease in the characteristic length scale, which in this case is the particle-to-particle distance. Moreover, the structure peak became sharper as the concentration increased, which indicates that the sample transitions to a more ordered structure, as mentioned previously. The relative peak position (q/q^*) did not reveal any ordered structure due to the low kinetics of the micelles at room temperature, which fail to reach the thermodynamically
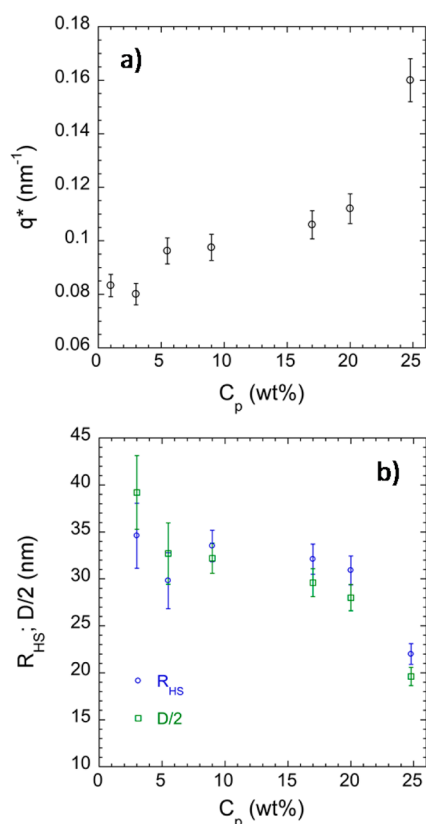
Figure 4. (a) Evolution of the position of the first structure peak (q^*) with polymer concentration. (b) Evolution of the effective hard sphere radius (R_{HS}) and the average center-to-center distance ($D/2$) with polymer concentrations from the PEO−PS−PEO/[BMIM][PF$_6$] system. D is obtained as $D = 2\pi/q^*$.

favorable state of a body-centered cubic (BCC) lattice as observed for PS−PEO−PS in the same IL at elevated temperatures.[30]

The change of the effective hard sphere radius (R_{HS}) as a function of polymer concentration is plotted in Figure 4b. This parameter remained constant at about 33 nm for concentrations up to 9 wt %. Above 9 wt %, R_{HS} decreased with increasing polymer concentration, indicating compression of the micellar shell and the formation of denser particles.

The evolution of the average of the center-to-center distance (expressed as $D/2$) between the micelles can also be extracted and is depicted in Figure 4b. D was obtained from the relative structure peak position at each concentration, such that $D = 2\pi/q^*$. Similarly to the evolution of R_{HS}, $D/2$ remained constant up to 9 wt % and decreased above this concentration, which indicates compression of the micellar corona. More importantly, at concentrations above the overlapping concentration c^*, D was smaller than $2R_{HS}$, which should be due to interpenetration between the corona chains of adjacent micelles.[52]

The evolution of the effective volume fraction with polymer concentration is shown in Figure 5. The volume fraction increased with increasing polymer concentration, reaching significantly high values (0.48) at the highest concentration studied (24.8 wt %), indicating that the system approaches the glass transition. The polymer concentration dependence of L^*_{app} is also shown in Figure 5. L^*_{app} is the size ratio between the coronal layer thickness and the core of the micelles (e.g., $L^*_{app} = (R_{HS} - R_c)/R_c$,[51] where $R_c = 10$ nm as described
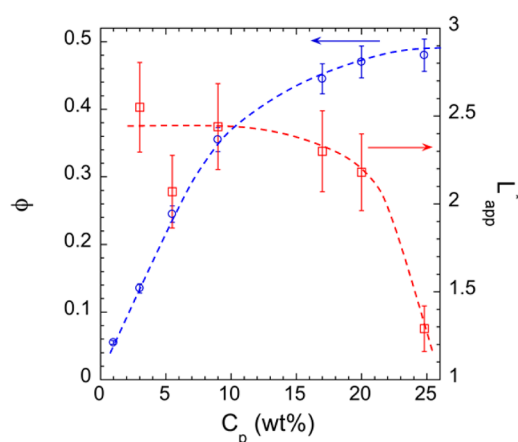
Figure 5. Evolution of φ and L^*_{app} with polymer concentrations of the PEO−PS−PEO/[BMIM][PF$_6$] system. Dotted lines are plotted as a guide for visualization of the trend.

above). It is well-known that for purely hard sphere systems $L^*_{app} \rightarrow 0$. The more this parameter deviates from 0, the softer the system becomes.[50] For block copolymer micelles, McConnell et al.[53] reported two different behaviors depending on the type of repulsive interactions occuring between the micelles. For small ratios of $L^*_{app} < 1.6$, the system behaved as a hard sphere showing face centered cubic structure, whereas for larger ratios a BCC structure was observed, indicating that soft repulsive interactions governed. As shown in Figure 5, the ratio of L^*_{app} is well above 1.6 at low concentrations, and the system thus presents an amorphous structure, as explained above. This parameter decreased with increasing concentration, approaching values close to those of hard sphere behavior. At the highest concentration studied (e.g., 24.8 wt %), L^*_{app} decreased to 1.3, indicating that the sample approaches hard sphere behavior.

Liquid to Soft Solid Transition and Rheological Properties. A number of polymer solutions with concentrations up to 25 wt % were prepared in [BMIM][PF$_6$], and their rheological behavior was first investigated by steady state shear flow experiments at room temperature. In Figure 6, viscosity profiles of various solutions are demonstrated as viscosity versus shear stress. At concentrations <3 wt %, a Newtonian behavior was observed, whereas at higher concentrations, the profile is characterized by a Newtonian plateau at low shear stresses followed by a shear thinning effect. Zero-shear viscosity (η_0), determined at the Newtonian plateau,
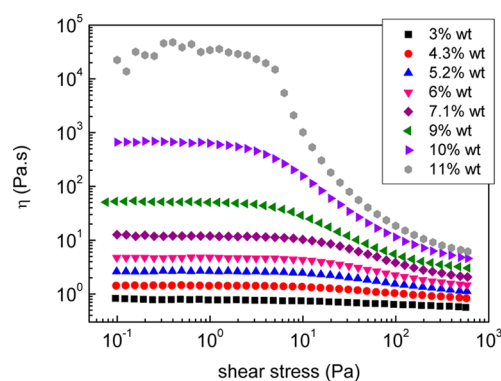

Figure 6. Steady state shear viscosity as a function of shear stress for different concentrations of the PEO−PS−PEO triblock copolymer dissolved in [BMIM][PF$_6$] at 25 °C.

increased while the critical shear stress, which marks the onset of shear thinning, decreased with increasing concentration. This behavior is typical of particle colloidal suspensions and has also been observed recently in a poly(methyl methacrylate)-grafted silica nanoparticle (PMMA-g-NP)/[EMIM][TFSA] system.[40]

The solutions were viscous up to 10 wt % above which a free-supporting gel was formed as observed by tilting the vials. For more concentrated solutions, the flow curves exhibited yield stress, and thus creep experiments were used to determine η_0. Measurements were performed in the linear viscoelastic regime. As shown in Figure 7, an abrupt change in the compliance $J_e(t)$
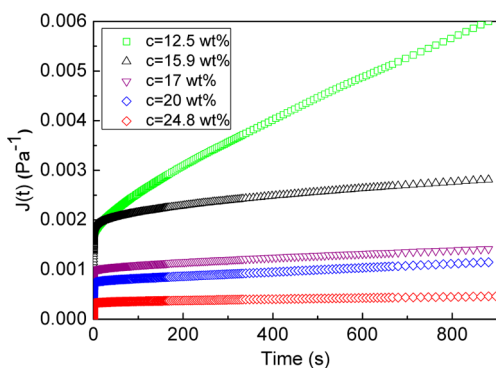

Figure 7. Creep compliance (J) as a function of time for different concentrations of PEO—PS—PEO in [BMIM][PF$_6$] at 25 °C.

was observed upon applying a sudden stress, followed by a smooth increase that becomes linear at longer time points. From the linear part of the plot of $J_e(t)$ over time, η_0 and the plateau modulus G_0 can be extracted according to the equation

$$J_e(t) = \frac{1}{G_0} + \frac{t}{\eta_0} \tag{8}$$

It can also be observed from Figure 7 that as the concentration increases the colloidal system tends to behave as an elastic solid, exhibiting very high viscosity and a high modulus ($1/J_e(t)$).

The variation in relative viscosity $\eta_{rel} = \eta_0/\eta_s$, where η_s is the viscosity of the solvent, as a function of concentration is demonstrated in Figure 8a. At low concentrations, the viscosity rises smoothly with concentration and becomes sharper when passing 4 wt %. Above the overlap concentration of the micellar nanoparticles, the viscosity diverges and a liquid to soft solid transition occurs. Crossover between the two regimes can be defined at 10 wt %. This is consistent with the fact that the suspensions at higher concentrations lose their ability to flow.

To compare the behavior of our system with that of other colloidal suspensions, we have plotted the data in a log—log plot of η_{rel} versus the normalized concentration $c/c*$ (Figure 8b), which is equivalent to the effective volume fraction (φ_{eff}) representing the volume fraction of effective spheres having a radius equal to the hydrodynamic radius of the micellar nanoparticles in the dilute regime.[54−56] Note that the φ_{eff} values are different than those extracted from SAXS (Figure 5), which take into account contraction of the shells.

In the same plot, data from the Krieger—Dougherty empirical equation (eq 9) describing the behavior of colloidal particles has been incorporated for the sake of comparison.[57]
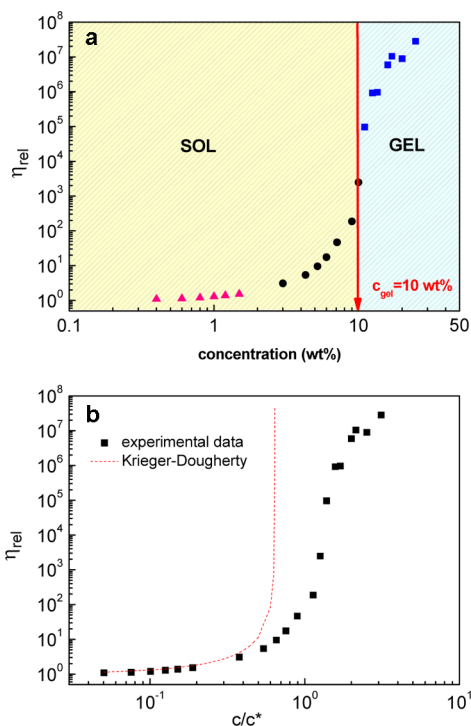

Figure 8. Log—log plot of the relative viscosity (η_{rel}) as a function of concentration (a) or normalized concentration $c/c*$ (φ_{eff}) (b) of the PEO—PS—PEO triblock copolymer in [BMIM][PF$_6$] at 25 °C. The symbols in (a) represent data obtained by microviscometer (▲), steady state shear (●), and creep (■) measurements. The red dashed line in (b) represents eq 10 with $\varphi_p = 0.64$.

$$\eta_{rel} = \left(1 - \frac{\varphi_{eff}}{\varphi_p}\right)^{-2.5\varphi_p} \tag{9}$$

where η_{rel} is the relative viscosity (η_0/η_s) and φ_p is the close-packing volume fraction of hard spheres. As shown in Figure 8b, the experimental data deviated from the hard sphere behavior predicted by eq 9 at $\varphi_p = 0.64$, the value for the random close-packing limit above which the viscosity diverges. It is observed that viscosity divergence of the micellar nanoparticle suspension occurs at a φ_{lim} that is remarkably higher than that of hard spheres due to their "soft" coronas, which allows for deformation and interpenetration of the PEO chains. Similar behavior has been observed for other "soft" nanoparticle suspensions (e.g., multiarm star polymers,[56,58] core—shell latexes,[59] grafted inorganic nanoparticles,[60] and microgels[61]). Comparing the results of the system under investigation with that of PMMA-g-NP in [EMIM][TFSA], we observe that the latter exhibits viscosity divergences at lower φ_{lim}, which should be attributed to less "softness" of PMMA-g-NP. This is in accordance with the fact that, with a silica core radius of 62 nm, the grafted silica nanoparticles exhibit $L*_{app}$ values in the range of 1−1.8,[40] which are considerably lower than that of our micellar nanoparticles, implying behavior that is much closer to that of hard spheres.

Oscillatory shear experiments were employed to explore the viscoelastic response of the micellar nanoparticle suspensions. Characteristic frequency sweep plots of the storage (G') and loss modules (G'') for several concentrations in the vicinity of the liquid soft solid transition, obtained in the linear viscoelastic regime, are presented in Figure 9. At $c = 9$ wt %, a nearly
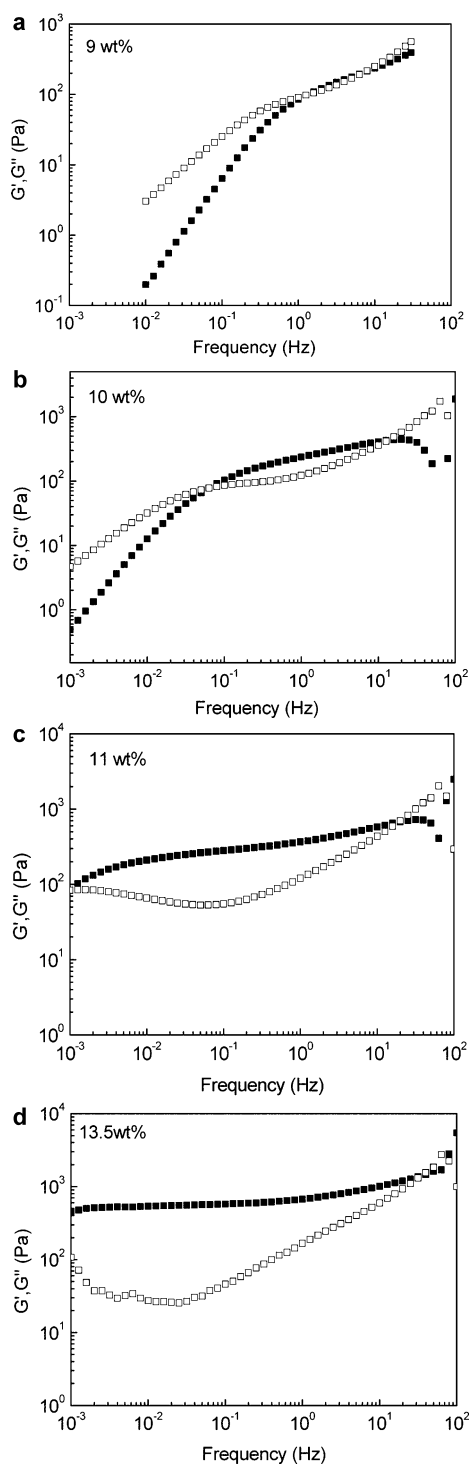
Figure 9. Frequency dependence of the dynamic shear moduli G' (closed symbols) and G'' (opened symbols) of the PEO−PS−PEO/[BMIM][PF$_6$] suspensions at different polymer concentrations at 25 °C.

liquidlike response was observed at low frequencies ($G' \sim \omega^2$, $G'' \sim \omega$), whereas G' almost coincides with G'' at higher frequencies, suggesting the vicinity of the transition. As the concentration increases, $G'(\omega)$ begins to dominate over a frequency window that broadens toward lower frequencies. It is also observed that $G'(\omega)$ develops a plateau that is nearly frequency independent at least in the low frequency range. On the other hand, $G''(\omega)$ is frequency dependent, exhibiting a

shallow minimum and at higher frequencies rising more sharply than $G'(\omega)$, ultimately exceeding it. This kind of viscoelastic response has been reported for colloidal uncoated silica hard spheres near and below the liquid−colloidal glass transition[60] and in other soft glassy colloidal systems.[16,17] Thus, we observed two relaxation modes: a slow one and a fast one, corresponding to low and high frequency crossover, respectively. The slow mode characteristic time (terminal relaxation time) increases steeply with concentrations >9 wt %, and the crossover frequency could not be observed by oscillatory measurements for concentrations >11 wt %. The high frequency crossover is weakly concentration dependent. A similar viscoelastic response (Figure 9d) was observed for the suspensions of concentrations >13.5 wt %.

From Figure 9, it is obvious that when the nanoparticle concentration is increased, the viscoelastic response of the system shows a liquid-to-solidlike transition marked by a dramatic increase in the terminal relaxation time and domination of the elastic modulus. In Figure 10a, the terminal
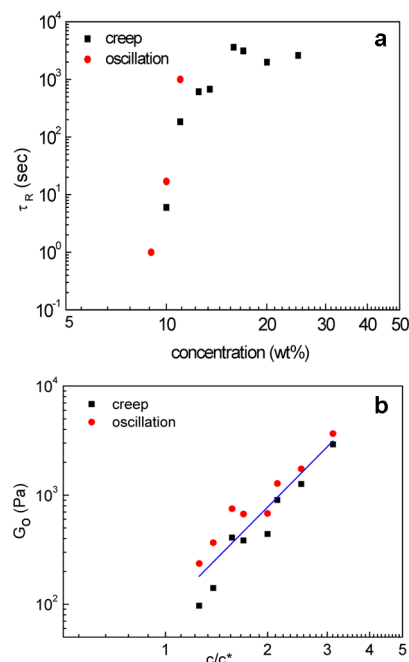

Figure 10. (a) Relaxation time (τ_R) and (b) plateau modulus (G_0) as a function of concentration and reduced concentration, respectively, of the PEO−PS−PEO/[BMIM][PF$_6$] system at 25 °C. The results ensued from dynamic oscillatory sweeps and the creep experiment.

relaxation time (τ_R) has been plotted as a function of concentration. In the same plot, values determined at higher concentrations by creep measurements ($\tau_R = G_0 \eta_0$, from Figure 7) have also been incorporated. As observed, τ_R increases by ∼3 orders of magnitude from 9 to 11 wt % and tends to level off at higher concentrations. These long relaxation times should be ascribed to the fact that the micellar nanoparticles are trapped in cages formed by their neighbors as crowding increases, producing a jamming effect.[53] The short relaxation times, on the order of tenths of seconds (fast mode), probably reflect localized motion of the individual nanoparticles.[62]

The plateau modulus G_0, as deduced from creep and oscillatory measurements, increased sharply with concentration. This accounts for the compression of the soft shell of the polymeric micelles and thus the decrease in the interparticle

distance observed by SAXS. Correlating the data from rheology and SAXS, we found a scaling behavior of the form $G' \cong D^{-2.7}$, provided that the aggregation number remained constant with concentration. The exponent -2.7 is close to that observed for other colloidal block copolymer systems in organic solvents (e.g., -2.46 for PS-P2VP in toluene[47]) and is not far from the theoretical prediction of $G' \cong N_{agg}^{3/2}D^{-2}$, derived from the repulsive potential obtained for polymerically stabilized colloidal nanoparticles.[63]

To estimate the micellar nanoparticle softness, we followed the procedure proposed by Paulin et al.[64] and applied it to the PMMA-g-NP/[EMIM][TFSA] system.[40] Figure 10b demonstrates G_0 as a function of $c/c*$ (equivalent to φ_{eff}) exhibiting low power dependence such that

$$G_0 \cong \varphi_{eff}{}^{m} \tag{10}$$

where $m = n/3 + 1$ with n being the soft interparticle potential. m was found to be 3.14, giving $n = 6.42$, which is lower than the values found in the PMMA-g-NP/[EMIM][TFSA] system. Thus, the PEO−PS−PEO nanoparticles seem to be softer than those of PMMA-g-NP, which is consistent with the fact that the viscosity diverges at higher φ_{eff} for the present system. However, the chain density of the PEO corona chains, which is about 0.14 chain/nm^2, is on the same order of magnitude as those reported for the PMMA grafting chains in PMMA-g-NP (0.11−0.2 chain/nm^2). Thus, the higher nanoparticle softness in the present system could be attributed to a thicker corona (as reflected by $L*_{app}$), which is more compressible, and a chain flexibility of PEO (low T_g, approximately -60 °C) that is much higher than that of PMMA (high T_g, $\sim$100 °C).

Thermal Stability. Lastly, to explore the thermal stability of the soft glassy solid formed by the jammed micellar nanoparticles, a preliminary test was accomplished using cone and plate geometry. The dynamic moduli were measured in a temperature sweep experiment at a constant strain of 1% (linear viscoelastic regime) and a frequency of 0.1 Hz. In Figure 11, G' and G'' are plotted versus temperature from 20 to 150
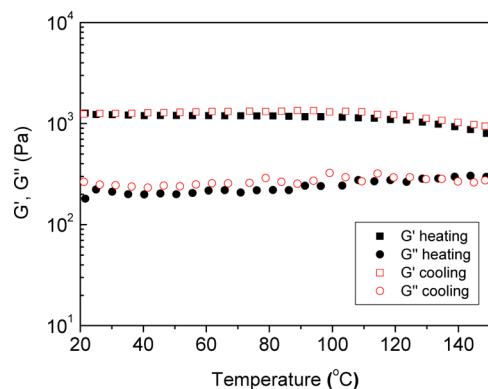

Figure 11. Temperature dependence of dynamic shear moduli (G' and G'') for 20 wt % PEO−PS−PEO in [BMIM][PF$_6$]. The measurements were taken with a cone and plate geometry at a strain (γ) of 1%, frequency of 0.1 Hz, and heating rate of 5 °C/min.

°C and then back to 20 °C for 20 wt % copolymer using a heating rate of 5 °C/min. As can be observed, the solidlike behavior of the suspension resists heating up to 150 °C practically without hysteresis. Moreover, the elastic modulus begins decreasing smoothly above 100 °C but remains higher than the loss modulus.

Subsequently, a more elaborate experiment was carried out using parallel plate geometry calibrated to minimize the effect of thermal expansion of the component dimensions at a lower heating rate of 1 °C/min.

In Figure 12, G' and G'' are plotted versus temperature from 20 to 160 °C for a 20 wt % copolymer. As observed, the elastic
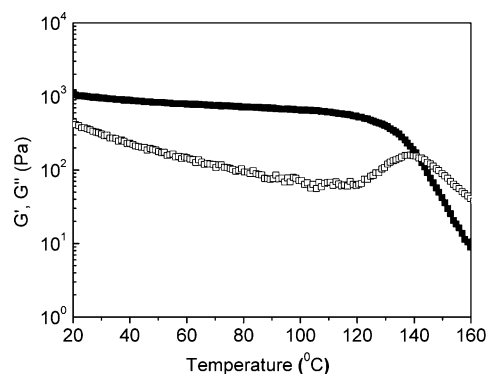

Figure 12. Temperature dependence of dynamic shear moduli G' and G'' for 20 wt % PEO−PS−PEO in [BMIM][PF$_6$]. Measurements were taken at a strain (γ) of 1%, frequency of 1 Hz, and heating rate of 1 °C/min.

modulus decreased smoothly up to 120 °C and was always significantly higher than G'', again indicating remarkable thermal stability of the material elasticity within this temperature range. However, a soft solid to liquid transition temperature, marked by crossing of the G' and G'' curves, was found at 141 °C, which was not observed using the faster heating rate in the previous experiment (Figure 11). Note that the experiments were performed in air, and the degradation of [BMIM][PF$_6$] was observed at the highest temperatures, which seems to agree with previous findings.[21,65]

As reported recently from experimental observations, PEO is soluble in [BMIM][PF$_6$] at room temperature up to at least 150 °C, implying an LCST that is higher than that in water,[67] which seems to be valid for other polymer/IL systems as well.[66,67] Thus, the observed soft solid to liquid transition should primarily be attributed to shrinkage of the PEO corona chains as they approach the LCST phase transition of PEO. The fact that this transition occurs above the T_g of PS ($\sim$100 °C) implies higher chain mobility of the PS segments in the core and thus an increase in the exchange dynamics that should lead to a "frozen" to dynamic micelle transition. Therefore, this effect is likely not the reason that the melting temperature is 141 °C, because otherwise it should manifest at a temperature closer to 100 °C.

■ CONCLUSIONS

In this work, the structural and rheological properties of concentrated solutions of a PEO−PS−PEO triblock copolymer in [BMIM][PF$_6$] ionic liquid are demonstrated. The copolymer self-assembles to form "frozen" micellar nanoparticles comprising a PS glassy core of nearly constant size over the concentration range investigated and a PEO swollen corona with high chain density. Upon increasing concentration, a liquid to soft solid transition was observed at $\varphi_{eff} = 1.25$ ($C_p = 10$ wt %), which is significantly higher than the $\varphi_{eff} = 0.64$ predicted for colloidal hard sphere suspensions. This behavior was mainly attributed to the "soft" nature of the corona of the polymeric nanoparticles allowing deformation and/or interpenetration of

PEO flexible chains. At elevated concentrations well above the liquid to solid transition, a nearly elastic soft solid was formed as revealed by creep and oscillatory flow experiments.

SAXS experiments did not show the appearance of any specific crystalline order (e.g., BCC) at room temperature, even at the highest concentration investigated (24.8 wt %), implying the formation of an amorphous glassy soft solid arising from the nanoparticle jamming. The structural parameters of the PEO–PS–PEO/[BMIM][PF$_6$] system exhibited remarkable changes upon increasing concentration in the solid phase (i.e., decreased hard sphere radius (R_{HS}) and interparticle distance (D), which was attributed to compression of the soft coronas and interpenetration of the dangling PEO chain ends). Inspection of the thermal response of the formed ion gel indicated remarkable thermal stability up to 120 °C and a melting temperature at 141 °C, which is among the highest observed to date in ion soft solids.[30,68]

We have presented an alternative method, aside from those of transient networks, to fabricate ion soft amorphous materials from core–shell-type block copolymer self-assemblies that jam at elevated polymer concentrations (Scheme 1). This physical

Scheme 1. Schematic Representation of the Solidification Process of Soft Polymeric Nanoparticles in Ionic Liquid: From Nanoparticle Suspension to Colloidal Glass
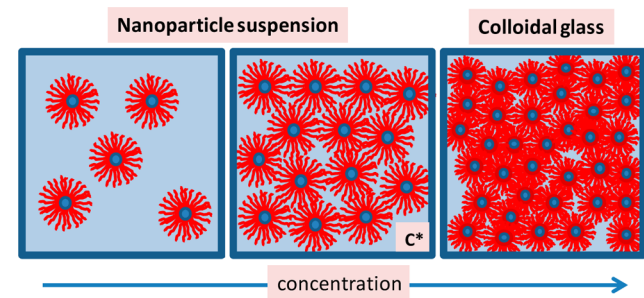
picture was verified by scanning electron microscopy. In Figure 13, a SEM micrograph obtained from a 20 wt % suspension embedded on a mica substrate is shown. Fortunately, some ion gel microdomains survived in the form of a thin film after rinsing with CH$_2$Cl$_2$, allowing us to reveal the jammed spherical

nanoparticles that form an amorphous structure. The characteristic sizes, that is, the particle core diameter and mean intermicellar distance, are in excellent agreement with those determined by SAXS.

To the best of our knowledge, this is the first study of glassy suspensions comprising polymeric soft nanoparticles in ionic liquids. The rheological properties of the ion soft solids formed were remarkably different from those observed in topologically reversed PEO–PS–PEO-based ion free supporting gels studied to date.[28,29] The properties and structural characteristics of the polymeric nanoparticle/IL suspensions could be tuned by designing copolymer characteristics (i.e., relative length of the solvophobic/solvophilic block) and polymer/IL interactions.

By combining properties of these kinds of soft solid formulations that have high viscosity and elastic modulus (e.g., 2.5×10^6 Pa s and 1.2×10^3 Pa, respectively, at 20 wt % polymer), negligible volatility of IL, high thermal stability, and easy tunability of the structural characteristics, several potential applications could be envisioned, particularly under working conditions requiring material integrity and high thermal stability (e.g., at elevated temperatures and/or reduced pressure). For instance, the above suspensions could be used as drilling fluids, replacing conventional media such as water or organic solvents.

More importantly, and because of the additional high conductivity of ILs, the easily shaped ion/gel described above might be a good candidate as a functional material for applications in electrochemical devices, including lithium ion batteries, fuel cells, and solar batteries.[69] Although we have not measured the ion conductivity of the present system, it is known that ion conductivity depends on the IL content, the block copolymer solvophilic content, and the nanostructure of the formulation (i.e., high IL content, high PEO length, and continuous microphase morphology are favorable). In previous findings with similar copolymers (PS-b-PEO), high ion conductivities have been measured (e.g., 0.8×10^{-2} S cm^{-1} for ionic content at 25 wt % and 100 °C).[70] In our system, the IL content and PEO length are remarkably higher, implying that much higher conductivities should be expected. Thus, it is reasonable to assume that our amorphous ion/gel, which provides continuous ionic domains, could meet the requirements for such applications.

■ ASSOCIATED CONTENT

Ⓢ Supporting Information

Experimental details on the ^{1}H NMR and GPC chromatogram of PEO–PS–PEO, fitting parameters for the SAXS experiments, and SEM micrographs from 20 wt % PEO–PS–PEO/[BMIM][PF$_6$] system. This material is available free of charge via the Internet at http://pubs.acs.org.

■ AUTHOR INFORMATION

Corresponding Author

*E-mail: ct@chemeng.upatras.gr. Fax: +30 2610 997266. Tel: +30 2610 969531.

Notes

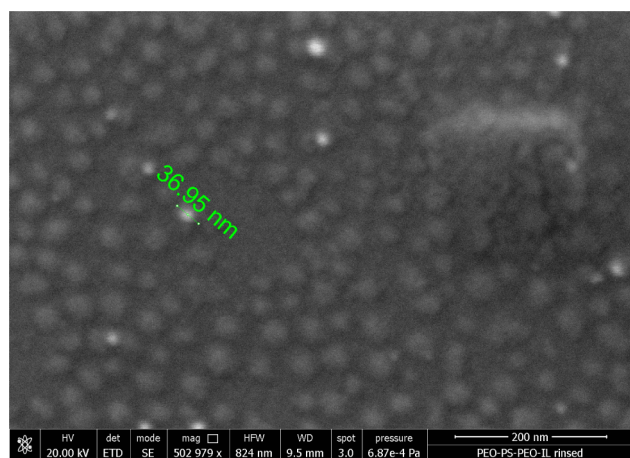The authors declare no competing financial interest.

Figure 13. SEM micrograph from 20 wt % PEO–PS–PEO suspended in [BMIM][PF$_6$] and embedded on a mica substrate that was preserved after rinsing with dichloromethane to remove the IL.

■ REFERENCES

(1) Alexandridis, P., Lindmann, B., Eds. *Amphiphilic Block Copolymers: Self-Assembly and Applications*; Elsevier: Amsterdam, The Netherlands, 2000.

(2) Bhatia, S. R.; Mourchid, A.; Joanicot, M. Block Copolymer Assembly to Control Fluid Rheology. *Curr. Opin. Colloid Interface Sci.* 2001, 6, 471−478.

(3) Vewer, D. A. Z.; Picchioni, F.; Broekhuis, A. A. Polymers for Enhanced Oil Recovery: A Paradigm for Structure−Property Relationship in Aqueous Solution. *Prog. Polym. Sci.* 2011, 36, 1558−1628.

(4) Peppas, N. A.; Hilt, Z.; Khademhosseini, A.; Langer, R. Hydrogels in Biology and Medicine: From Molecular Principles to Bionanotechnology. *Adv. Mater. (Weinheim, Ger.)* 2006, 18, 1345−1360.

(5) Lee, K. Y.; Mooney, D. J. Hydrogels for Tissue Engineering. *Chem. Rev.* 2001, 101, 1869−1879.

(6) Rubinstein, M.; Dobrynin, A. Associations Leading to Formation of Reversible Networks and Gels. *Curr. Opin. Colloid Interface Sci.* 1999, 4, 83−87.

(7) Tsitsilianis, C. Responsive Reversible Hydrogels from Associative "Smart" Macromolecules. *Soft Matter* 2010, 6, 2372−2388.

(8) Kopeček, J. Hydrogel Biomaterials: A Smart Future? *Biomaterials* 2007, 28, 5185−5192.

(9) Jeong, B.; Kim, S. W.; Bae, Y. H. Thermosensitive Sol−Gel Reversible Hydrogels. *Adv. Drug Delivery Rev.* 2002, 54, 37−51.

(10) Liu, A. J.; Nagel, S. R. Nonlinear Dynamics: Jamming Is Not Just Cool Any More. *Nature* 1998, 396, 21.

(11) Mewis, J.; D'Haene, P. Prediction of Rheological Properties in Polymer Colloids. *Makromol. Chem., Macromol. Symp.* 1993, 68, 213−225.

(12) Hamley, I. W.; Daniel, C.; Mingvanish, W.; Mai, S. M.; Booth, C.; Messe, L.; Ryan, A. J. From Hard Spheres to Soft Spheres: The Effect of Copolymer Composition on the Structure of Micellar Cubic Phases Formed by Diblock Copolymers in Aqueous Solution. *Langmuir* 2000, 16, 2508−2514.

(13) Wang, P.; Zakeeruddin, S. M.; Comte, P.; Exnar, I.; Gratzel, M. Gelation of Ionic Liquid-Based Electrolytes with Silica Nanoparticles for Quasi-Solid-State Dye-Sensitized Solar Cells. *J. Am. Chem. Soc.* 2003, 125, 1166−1167.

(14) Vlassopoulos, D. Colloidal Star Polymers: Models for Studying Dynamically Arrested States in Soft Matter. *J. Polym. Sci., Part B: Polym. Phys.* 2004, 42, 2931−2941.

(15) Cloitre, M.; Borrega, R.; Monti, F.; Leibler, L. Structure and Flow of Polyelectrolyte Microgels: From Suspensions to Glasses. *C. R. Phys.* 2003, 4, 221−230.

(16) Derec, C.; Ducouret, G.; Ajdari, A.; Lequeux, F. Aging and Nonlinear Rheology in Suspensions of Polyethylene Oxide−Protected Silica Particles. *Phys. Rev. E: Stat., Nonlinear, Soft Matter Phys.* 2003, 67, 061403.

(17) Pham, K. N.; Petekidis, G.; Vlassopoulos, D.; Egelhaaf, S. U.; Poon, W. C. K.; Pusey, P. N. Yielding Behavior of Repulsion- and Attraction-Dominated Colloidal Glasses. *J. Rheol. (Melville, NY, U.S.)* 2008, 52, 649−676.

(18) Welton, T. Room-Temperature Ionic Liquids. Solvents for Synthesis and Catalysis. *Chem. Rev.* 1999, 99, 2071−2084.

(19) Wasserscheid, P.; Keim, W. Ionic Liquids: New "Solutions" for Transition Metal Catalysis. *Angew. Chem., Int. Ed.* 2000, 39, 3772−3789.

(20) Wilkes, J. S. A Short History of Ionic Liquids: From Molten Salts to Neoteric Solvents. *Green Chem.* 2002, 4, 73−80.

(21) Singh, M. P.; Singh, R. K.; Shandra, S. Ionic Liquid Confined in Porous Matrices: Physicochemical Properties and Applications. *Prog. Mater. Sci.* 2014, 64, 73−120.

(22) Ohno, H. *Electrochemical Aspects of Ionic Liquids*; Wiley-Interscience: New York, 2005.

(23) Cho, J. H.; Lee, J.; Xia, Y.; Kim, B.; He, Y.; Renn, M. J.; Lodge, T. P.; Frisbie, D. C. Printable Ion-Gel Gate Dielectrics for Low-Voltage Polymer Thin-Film Transistors on Plastic. *Nat. Mater.* 2008, 7, 900−906.

(24) Galinski, M.; Lewandowski, A.; Stepniak, I. Ionic Liquids as Electrolytes. *Electrochim. Acta* 2006, 51, 5567−5580.

(25) Matyjaszewski, K., Gnanou, Y., Leibler, L., Eds. *Macromolecular Engineering: Precise Synthesis, Materials Properties, Applications*; Wiley-VCH: Weinheim, Germany, 2007.

(26) Ueki, T.; Watanabe, M. Macromolecules in Ionic Liquids: Progress, Challenges, and Opportunities. *Macromolecules* 2008, 41, 3739−3749.

(27) Lu, J.; Yan, F.; Texter, J. Advanced Applications of Ionic Liquids in Polymer Science. *Prog. Polym. Sci.* 2009, 34, 431−448.

(28) He, Y.; Boswell, P. G.; Bühlmann, P.; Lodge, T. P. Ion Gels by Self-Assembly of a Triblock Copolymer in an Ionic Liquid. *J. Phys. Chem. B* 2007, 111, 4645−4652.

(29) Zhang, S.; Lee, K. H.; Frisbie, C. D.; Lodge, T. P. Ionic Conductivity, Capacitance, and Viscoelastic Properties of Block Copolymer-Based Ion Gels. *Macromolecules* 2011, 44, 940−949.

(30) Zhang, S.; Lee, K. H.; Sun, J.; Frisbie, C. D.; Lodge, T. P. Viscoelastic Properties, Ionic Conductivity, and Materials Design Considerations for Poly(styrene-*b*-ethylene oxide-*b*-styrene)-Based Ion Gel Electrolytes. *Macromolecules* 2011, 44, 8981−8989.

(31) Imaizumi, S.; Kokubo, H.; Watanabe, M. Polymer Actuators Using Ion-Gel Electrolytes Prepared by Self-Assembly of ABA-Triblock Copolymers. *Macromolecules* 2012, 45, 401−409.

(32) He, Y.; Lodge, T. P. A Thermoreversible Ion Gel by Triblock Copolymer Self-Assembly in an Ionic Liquid. *Chem. Commun. (Cambridge, U.K.)* 2007, 43, 2732−2734.

(33) He, Y.; Lodge, T. P. Thermoreversible Ion Gels with Tunable Melting Temperatures from Triblock and Pentablock Copolymers. *Macromolecules* 2008, 41, 167−174.

(34) Kitazawa, Y.; Ueki, T.; Niitsuma, K.; Imaizumi, S.; Lodge, T. P.; Watanabe, M. Thermoreversible High-Temperature Gelation of an Ionic Liquid with Poly(benzyl methacrylate-*b*-methyl methacrylate-*b*-benzyl methacrylate) Triblock Copolymer. *Soft Matter* 2012, 8, 8067−8074.

(35) Lu, J.; Yan, F.; Texter, J. Advanced Applications of Ionic Liquids in Polymer Science. *Prog. Polym. Sci.* 2009, 34, 431−448.

(36) Lee, J.; Panzer, M. J.; He, Y.; Lodge, T. P.; Frisbie, C. D. Ion Gel Gated Polymer Thin-Film Transistors. *J. Am. Chem. Soc.* 2007, 129, 4532−4533.

(37) Cho, J. H.; Lee, J.; Xia, Y.; Kim, B.; He, Y.; Renn, M. J.; Lodge, T. P.; Frisbie, C. D. Printable Ion-Gel Gate Dielectrics for Low-Voltage Polymer Thin-Film Transistors on Plastic. *Nat. Mater.* 2008, 7, 900−906.

(38) Lee, K. H.; Zhang, S.; Gu, Y.; Lodge, T. P.; Frisbie, C. D. Transfer Printing of Thermoreversible Ion Gels for Flexible Electronics. *ACS Appl. Mater. Interfaces* 2013, 5, 9522−9527.

(39) Ueno, K.; Inaba, A.; Sano, Y.; Kondoh, M.; Watanabe, M. A Soft Glassy Colloidal Array in Ionic Liquid, which Exhibits Homogeneous, Non-Brilliant and Angle-Independent Structural Colours. *Chem. Commun. (Cambridge, U.K.)* 2009, 3603−3605.

(40) Ueno, K.; Sano, Y.; Inaba, A.; Kondoh, M.; Watanabe, M. Soft Glassy Colloidal Arrays in an Ionic Liquid: Colloidal Glass Transition, Ionic Transport, and Structural Color in Relation to Microstructure. *J. Phys. Chem. B* 2010, 114, 13095−13103.

(41) Ueno, K.; Inaba, A.; Ueki, T.; Kondoh, M.; Watanabe, M. Thermosensitive, Soft Glassy and Structural Colored Colloidal Array in Ionic Liquid: Colloidal Glass to Gel Transition. *Langmuir* 2010, 26, 18031−18038.

(42) Kahveci, M. U.; Yagci, Y.; Avgeropoulos, A.; Tsitsilianis, C. Well-Defined Block Copolymers. In *Polymer Science: A Comprehensive Reference*; Müller, A. H. E., Wooley, K. L., Eds; Elsevier: Amsterdam, The Netherlands, 2012; Vol. 6, pp 455−509.

(43) Fedors, R. F. An Equation Suitable for Describing the Viscosity of Dilute to Moderately Concentrated Polymer Solutions. *Polymer* **1979**, *20*, 225−228.

(44) Guinier, A., Fournet, G., Eds. *Small-Angle Scattering of X-Rays*; John Wiley and Sons: New York, 1955.

(45) Percus, J. K.; Yevick, J. Analysis of Classical Statistical Mechanics by Means of Collective Coordinates. *Phys. Rev.* **1958**, *110*, 1.

(46) Ma, J.; Liang, B.; Cui, P.; Dai, H.; Huang, R. Dilute Solution Properties of Hydrophobically Associating Polyacrylamide: Fitted by Different Equations. *Polymer* **2003**, *44*, 1281−1286.

(47) Hourdet, D.; Ducouret, G.; Varghese, S.; Badiger, M. V.; Wadgaonkar, P. P. Thermodynamic Behavior of Hydrophobically Modified Polyacrylamide Containing Random Distribution of Hydrophobes: Experimental and Theoretical Investigations. *Polymer* **2013**, *54*, 2676−2689.

(48) Asai, H.; Fujii, K.; Ueki, T.; Sakai, T.; Chung, U.; Watanabe, M.; Han, Y.-S.; Kim, T.-H.; Shibayama, M. Structural Analysis of High Performance Ion-Gel Comprising Tetra-PEG Network. *Macromolecules* **2012**, *45*, 3902−3909.

(49) Lemmers, M.; Voets, I. K.; Cohen Stuart, M. A.; van der Gucht, J. Transient Network Topology of Interconnected Polyelectrolyte Complex Micelles. *Soft Matter* **2011**, *7*, 1378−1389.

(50) Buitenhuis, J.; Förster, S. Block Copolymer Micelles: Viscoelasticity and Interaction Potential of Soft Spheres. *J. Chem. Phys.* **1997**, *107*, 262−272.

(51) Voulgaris, D.; Tsitsilianis, C.; Grayer, V.; Esselink, E.; Hadziioannou, G. Amphiphile Micelles Formed by Polystyrene/Poly(vinyl-2-pyridine) Heteroarm Star Copolymers in Toluene. *Polymer* **1999**, *40*, 5879−5889.

(52) Loppinet, B.; Stiakakis, E.; Vlassopoulos, D.; Fytas, G.; Roovers, J. Reversible Thermal Gelation in Star Polymers: An Alternative Route to Jamming of Soft Matter. *Macromolecules* **2001**, *34*, 8216−8223.

(53) McConnell, G. A.; Gast, A. P.; Huang, J. S.; Smith, S. D. Disorder-Order Transitions in Soft Sphere Polymer Micelles. *Phys. Rev. Lett.* **1993**, *71*, 2102−2105.

(54) Asteriadi, A.; Sigel, R.; Vlassopoulos, D.; Meier, G.; Dorgan, J. R.; Knauss, D. M. Molecular Control of the Viscosity of Model Dendritically Branched Polystyrene Solutions: From Polymeric to Colloidal Behavior. *Macromolecules* **2004**, *37*, 1016−1022.

(55) Roovers, J. Concentration Dependence of the Relative Viscosity of Star Polymers. *Macromolecules* **1994**, *27*, 5359−5364.

(56) Goh, T. K.; Coventry, K. D.; Blencowe, A.; Qiao, G. G. Rheology of Core Cross-Linked Star Polymers. *Polymer* **2008**, *49*, 5095−5104.

(57) Krieger, I. M.; Dougherty, T. J. A Mechanism for Non-Newtonian Flow in Suspensions of Rigid Spheres. *Trans. Soc. Rheol.* **1959**, *3*, 137−152.

(58) Vlassopoulos, D.; Fytas, G.; Pispas, S.; Hadjichristidis, N. Spherical Polymeric Brushes Viewed as Soft Colloidal Particles: Zero-Shear Viscosity. *Phys. B (Amsterdam, Neth.)* **2001**, *296*, 184−189.

(59) Senff, H.; Richtering, W.; Norhausen, C.; Weiss, A.; Ballauff, M. Rheology of a Temperature Sensitive Core−Shell Latex. *Langmuir* **1999**, *15*, 102−106.

(60) McEwan, M.; Green, D. Rheological Impacts of Particle Softness on Wetted Polymer-Grafted Silica Nanoparticles in Polymer Melts. *Soft Matter* **2009**, *5*, 1705−1716.

(61) Tan, B. H.; Tam, K. C.; Lam, Y. C.; Tan, C. B. Microstructure and Rheological Properties of pH-Responsive Core−Shell Particles. *Polymer* **2005**, *46*, 10066−10076.

(62) Mason, T. E.; Weitz, D. A. Linear Viscoelasticity of Colloidal Hard Sphere Suspensions near the Glass Transition. *Phys. Rev. Lett.* **1995**, *75*, 2770−2773.

(63) Witten, T. A.; Pincus, P. A. Colloid Stabilization by Long Grafted Polymers. *Macromolecules* **1986**, *19*, 2509−2513.

(64) Paulin, S. E.; Ackerson, B. J.; Wolfe, M. S. Equilibrium and Shear Induced Nonequilibrium Phase Behavior of PMMA Microgel Spheres. *J. Colloid Interface Sci.* **1996**, *178*, 251−262.

(65) Singh, M. P.; Singh, R. K.; Shandra, S. Thermal Stability of Ionic Liquid in Confined Geometry. *J. Phys. D: Appl. Phys.* **2010**, *43*, 092001.

(66) Lee, H.-N.; Lodge, T. P. Lower Critical Solution Temperature (LCST) Phase Behavior of Poly(ethylene oxide) in Ionic Liquids. *J. Phys. Chem. Lett.* **2010**, *1*, 1962−1966.

(67) Lee, H.-N.; Newell, N.; Bai, Z.; Lodge, T. P. Unusual Lower Critical Solution Temperature Phase Behavior of Poly(ethylene oxide) in Ionic Liquids. *Macromolecules* **2012**, *45*, 3627−3633.

(68) Nagasawa, J.; Matsumoto, H.; Yoshida, M. Highly Efficient and Specific Gelation of Ionic Liquids by Polymeric Electrolytes to Form Ionogels with Substantially High Gel−Sol Transition Temperatures and Rheological Properties like Self-Standing Ability and Rapid Recovery. *ACS Macro Lett.* **2012**, *1*, 1108−1112.

(69) Ye, Y.-S.; Rick, J.; Hwang, B.-J. Ionic Liquid Polymer Electrolytes. *J. Mater. Chem. A* **2013**, *1*, 2719−2743.

(70) Simone, P. M.; Lodge, T. P. Phase Behavior and Ionic Conductivity of Concentrated Solutions of Polystyrene-Poly(ethylene oxide) Diblock Copolymers in an Ionic Liquid. *ACS Appl. Mater. Interfaces* **2009**, *1*, 2812−1820.